Theoretical and experimental study on a compliant flipper-leg during terrestrial locomotion

2016 Bioinspir. Biomim. 11 056005

(http://iopscience.iop.org/1748-3190/11/5/056005)

Bioinspiration & Biomimetics

PAPER

Theoretical and experimental study on a compliant flipper-leg during terrestrial locomotion

Tao Fang[1], Youcheng Zhou[1], Shikun Li[2], Min Xu[1], Haiyi Liang[2], Weihua Li[3] and Shiwu Zhang[1]

[1] Department of Precision Machinery and Precision Instrumentation, University of Science and Technology of China, Hefei, Anhui, 230026, People's Republic of China
[2] Department of Modern Mechanics, University of Science and Technology of China, Hefei, Anhui, 230026, People's Republic of China
[3] School of Mechanical, Materials and Mechatronic Engineering, University of Wollongong, Wollongong, NSW 2522, Australia

E-mail: swzhang@ustc.edu.cn

RECEIVED
13 April 2016

REVISED
16 June 2016

ACCEPTED FOR PUBLICATION
20 July 2016

PUBLISHED
17 August 2016

Keywords: compliant flipper-leg, amphibious robot, mechanical analysis, single-leg platform, four-leg-robot platform

Abstract

An amphibious robot with straight compliant flipper-legs can conquer various amphibious environments. The robot can rotate its flipper-legs and utilize their large deflection to walk on rough terrain, and it can oscillate the straight flipper-legs to propel itself underwater. This paper focuses on the dynamics of the compliant straight flipper-legs during terrestrial locomotion by modeling its deformation dynamically with large deflection theory and simulating it to investigate the parameters of locomotion such as trajectory, velocity, and propulsion. To validate the theoretical model of dynamic locomotion, a single-leg experimental platform is used to explore the flipper-legs in motion with various structural and kinematic parameters. Furthermore, a robotic platform mounting with four compliant flipper-legs is also developed and used to experiment with locomotion. The trajectories of the rotating axle of the compliant flipper-leg during locomotion were approximately coincidental in simulation and in experiments. The speed of locomotion and cost of transport during locomotion were explored and analyzed. The performance of different types of compliant flipper-legs during locomotion shows that varying the degrees of stiffness will have a significant effect on their locomotion. The dynamic model and analysis of the compliant flipper-leg for terrestrial locomotion facilitates the ability of amphibious robots to conquer complex environments.

1. Introduction

Amphibious robots perform important roles in many civilian and military applications such as navigation shores, clearing mines and mapping terrain [1]. However, different types of amphibious robots have been developed for different roles, such as salamander-like robot [2, 3], ACM series robots [4], and turtle-like robots [5]. To improve their performance in terrestrial and underwater tasks, amphibious robots need to be stable and able to adapt to various terrains and water environments. Nowadays, researchers are proposing approaches that will enable robots to smoothly and efficiently switch between different operational modes on terrestrial and aquatic environments. We have developed an actively transformable flipper-leg capable of swimming under water and walking on terrain, and an amphibious robot—AmphiHex-I where the mechanism is a propulsion unit that has been assembled and implemented [6–8]. AmphiHex-I has six flipper-legs with embedded steel plates and cables that can transform the flipper-legs between straight flippers and curved legs by loosening or tightening the cables. However, this active transformation needs extra motors to move the cables, which increases the complexity of the control strategy and driving modules. Hence, a simpler mechanism of transformable propulsion for the amphibious robot is needed for field applications.

Many other robots, a s well as AmphiHex-I use soft structures for the propulsion unit and the connector or body, such as the arms of an octopus-like robot or compliant joints in artificial fingers, softworms [9–11]. Inspired by these soft structures, we developed a compliant flipper-leg that can act as the propulsion unit. This compliant flipper-leg is designed as a straight plate made from an elastic material that can be transformed passively [12]. This flipper-leg can propel

the robot underwater like turtle's flippers, and also bend to a curved shape for terrestrial locomotion when normal and tangential forces exerted by different terrains applied. Thus, this compliant flipper-leg has a similar function as AmphiHex-I, and thus has a simpler structure, a simplified driving module, and an easier control strategy.

This flipper-leg has a two-fold compliance: (1) it can be used as a flipper and oscillate to propel underwater, and (2) it can bend into a curved leg during locomotion on different terrain. Compliant flippers mounted on robots as propulsion units to mimic animal flippers has been applied and verified in many underwater robots [13–16]. However, the ability of straight compliant flipper-legs to propel an amphibious robot on different terrain still needs further work.

Exploring the interaction between the propulsion unit and the environment help understand the dynamics of the robot and guide the design and the control of the field robot [17–20]. The dynamics of a compliant flipper-leg must be examined in order to understand their propulsive ability on different terrains. However, modeling the dynamics of a compliant flipper-leg means simplifying its deformation and the complex interaction between the flipper-leg and terrain. This deformation is difficult to model due to its nonlinearity and multi- dimensionality. Aribert has contributed a great deal to the analysis and application of compliant legs [21] by focusing on compliant legs that mainly consist of rigid and soft parts that have theoretically proved to be stable, controllable, and efficient due to compliance [22]. Since a compliant leg made from soft material, as a pseudo rigid body model (PRBM), has proved a successful way of modeling a compliant beam with large deflections [23–25], PRBM regards a compliant beam as a combination of two rigid bars and a torque spring set at a suitable position, while neglecting any nonlinearity of the material in large deformations. As with PRBM, PRBM 3R divides a compliant beam into three rotating springs and four bars that results in a more accurate but more complex model than PRBM [26]. A rolling spring loaded inverted pendulum is suitable for curved-leg, like that of RHex, because it divides the leg into a straight rigid bar, a curved rigid bar, and a rotating spring [27, 28]. However, it is hard to derive an explicit solution because these theoretical models are too complex, so finite element analysis is a good choice to cover mechanical problems that include a credible nonlinearity and the complex interaction of parts with each other [29, 30].

In this paper we aim to explore the feasibility and performance of a compliant flipper-leg during locomotion on terrain by theoretical modeling and experimental validation. We used large deflection equations once used to verify PRBM, to model the compliant leg, and set up a finite element model to simulate the entire motion of the leg to obtain more parameters. With these methods, we can explore movements such as forward speed, fluctuations in height, propulsion efficiency, and the design of the compliant legs. The theoretical results were validated by experiments with moving platform, and moving robots. This study facilitates implementing amphibious robots to conquer various complex environments.

The reminder of the paper is organized as follows. Section 2 introduces the leg locomotion platform, the theoretical model of the compliant flipper-leg, and the robot locomotion platform. Section 3 presents the performance of propulsion from simulation and experiment, the special design of the compliant legs, and section 4 presents the conclusion.

2. Experimental system and mechanical model

In order to explore the feasibility and performance of straight compliant leg moving over terrain, we developed a single-leg locomotion platform, a theoretical model of the compliant leg, and a robot locomotion platform to conduct a theoretical and experimental analysis.

2.1. Single-leg locomotion platform

A single-leg locomotion platform was developed to explore the movement of compliant flipper-legs. Figure 1(a) shows a simplified draft of the locomotion platform; it consists of a horizontal cylindrical slide, two vertical cylindrical slides, a vertical displacement sensor, and a locomotion unit. The cylindrical slides provide horizontal and vertical translational freedoms for the locomotion unit; the propulsion unit also includes a driving unit and a compliant flipper-leg. The leg is made from polyurethane, which is widely used as a super elastic material. The driving unit contains a MAXON motor to drive the flipper-leg, a gear box, and a torque sensor, and the coordinate is set at the center of the flipper-leg's rotation. Figure 1(b) is a series of photographs of the leg during terrestrial motion. The red pointer at the front of the drive unit is used to measure the angle of rotation of the flipper-leg. The MAXON motor is controlled to vary the speed of rotation in a clockwise direction, and a weight is used to adjust the payload of the driving unit. The load applied vertically to the compliant leg is 2 kg, and 12.36 kg applied horizontally. The vertical load means the weight of a driving unit capable of moving in a vertical direction, while the horizontal load includes two vertical slide ways, two horizontal slide ways, and the driving unit and sensors that can move in a horizontal direction. The leg is 310 mm long x 55 mm wide x 15 mm deep; the leg weighs 76.7 g and Young's module is 25 Mpa.

The process by which the compliant leg is propelled on the locomotion platform is shown in

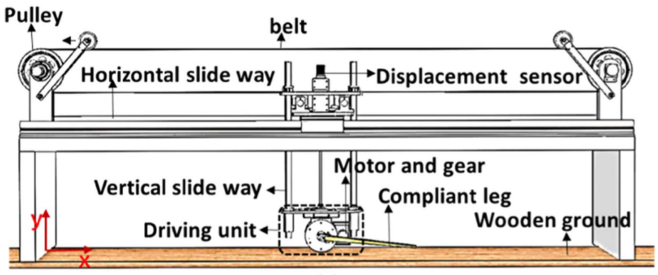

(a)

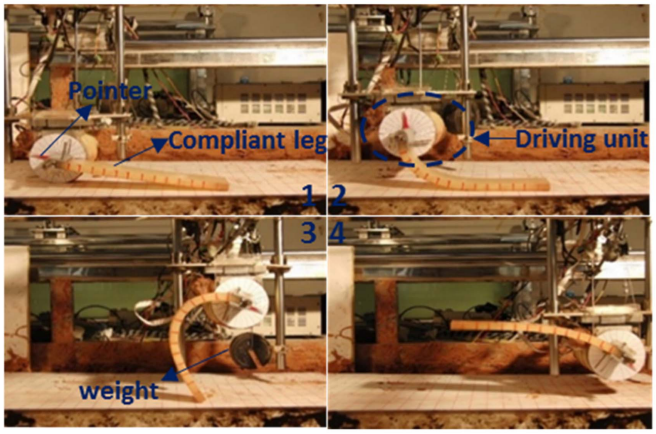

(b)

Figure 1. Single-leg locomotion platform. (a) Draft of the locomotion platform. (b) Snapshots of the compliant leg during one cycle in locomotion.

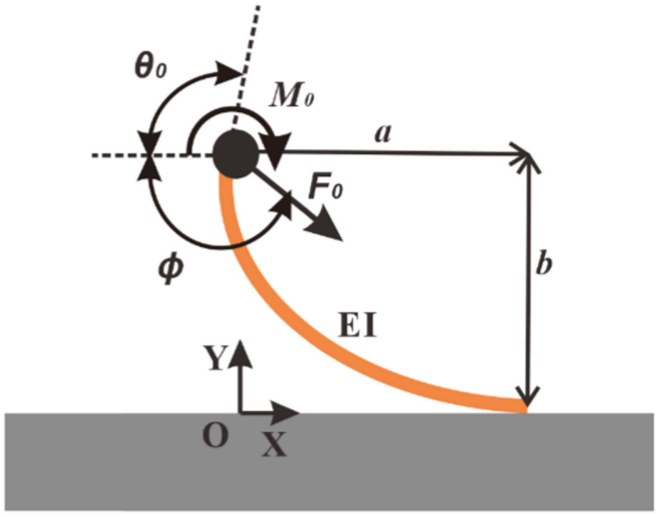

Figure 2. Diagram of large deflection cantilever's mechanical model.

figure 1(b). Here the leg is straight (see figures 1(b)(1)), but when the driving unit starts the leg bends into a curved shape under the driving load (see figure 1(b)(2)), while the driving unit is pushed forward by the flipper-leg. When the flipper-leg leaves the ground the driving unit drops down freely (see figures 1(b)(3) and (b)(4)). During locomotion, the flipper-leg bends continuously, an action that determines how well the propulsive unit can move itself along the platform.

2.2. Model of compliant flipper-leg

In PRBM or similar models, transforming part of the leg to be analyzed is simplified into bars of fixed lengths with torsion springs, but the length of that part of the flipper-leg that contacts the ground varies, which means the length of the bent part also varies; this means that modeling the leg as two bars with fixed lengths and rotation spring in a fixed position is very difficult, so the transforming part of the leg is regarded

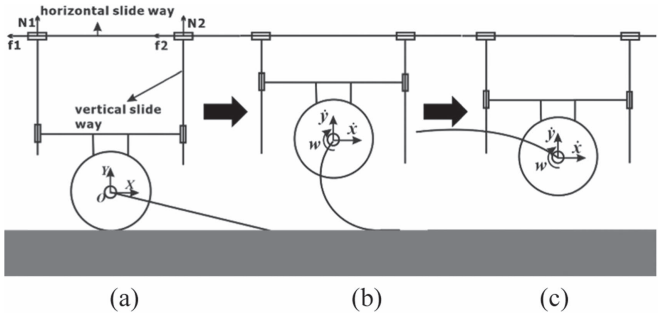

Figure 3. Three phases of the motion during one cycle of locomotion.

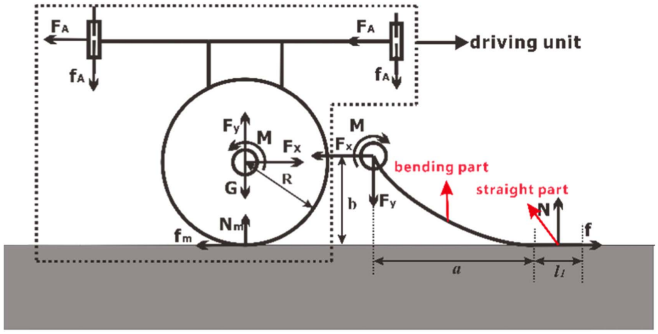

Figure 4. Diagram of the system before the driving unit leaves the ground (bending phase).

as a cantilever capable of large deflection, as shown in figure 2.

Thus, we can model the deflection of the leg with an implicit method that can be incorporated into three large deflection equations as shown below, which are derived from elastic theories and used to validate pseud rigid body model [23, 24]

$$l_2\sqrt{F_0/2EI} = \frac{1}{2}\int_0^{\theta_0} \times \frac{\mathrm{d}\theta}{\sqrt{[\cos(\theta_0+\Phi) - \cos(\theta+\Phi)] + M_o{}^2/2EIF_0}}, \quad (1)$$

$$a = \frac{1}{2\sqrt{F_0/2EI}}\int_0^{\theta_0} \times \frac{\cos(\theta)\mathrm{d}\theta}{\sqrt{[\cos(\theta_0+\Phi) - \cos(\theta+\Phi)] + M_o{}^2/2EIF_0}}, \quad (2)$$

$$b = \frac{1}{2\sqrt{F_0/2EI}}\int_0^{\theta_0} \times \frac{\sin(\theta)\mathrm{d}\theta}{\sqrt{[\cos(\theta_0+\Phi) - \cos(\theta+\Phi)] + M_o{}^2/2EIF_0}}, \quad (3)$$

where a and b denote the x-direction and y-direction displacements. θ_0 denotes the angle of tangential vector at the end of the flipper-leg. F_0 and M_0 denote the force and moment applied to the rotating tip, respectively. φ is the direction of F_0. l_2 denotes the length of the bent compliant flipper-leg. E is Young's modulus of the leg and I is the moment of inertia of the leg's cross section. Here we classified six independent variables into two groups, where the variables in the first group are a, b, and θ_0, which stand for the posture and position of the end of the compliant leg; the variables in the second group include F_0, M_0 and φ, which stand for the load applied to the compliant leg. In these equations there are six independent variables, so more equations are needed as boundary conditions to obtain a solution, albeit the three equations could be solved with boundary conditions by numerical method because they are implicit.

2.3. Model of single-leg locomotion platform

As mentioned above, since the number of the independent variables is six, more equations are needed to obtain a solution for leg deformation. Here we considered the locomotion platform of a single compliant flipper-leg to model the interactions between the flipper-leg, the driving unit, and the ground. To obtain the boundary conditions during locomotion the motion of the compliant flipper-leg was divided into three phases, as shown in figure 3; the bending phase, the lifting phase, and the flying phase. In the bending phase the compliant leg begins to bend, and the driving unit is always in contact with the ground. In the lifting phase the driving unit begins to leave the ground while the surface beneath the leg is

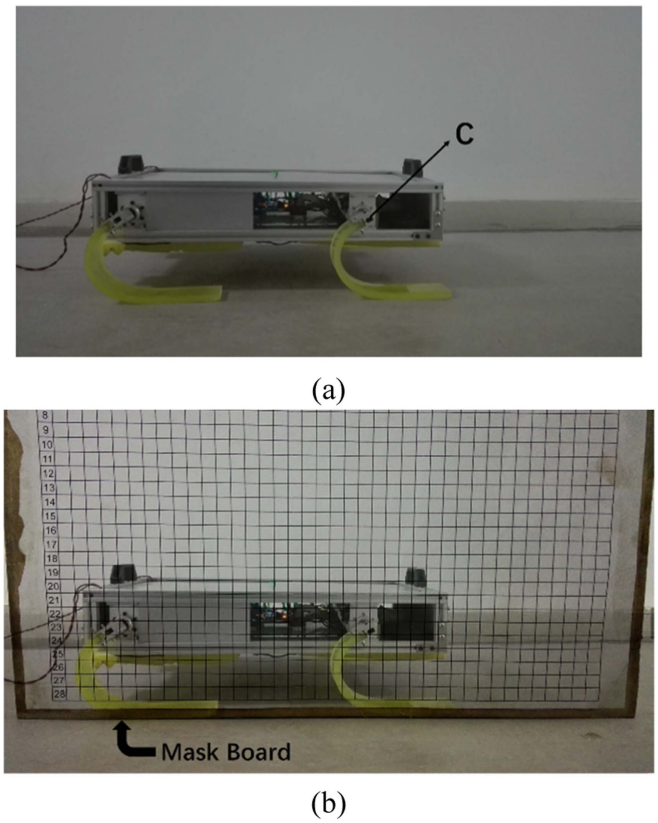

Figure 5. Four-leg-robot locomotion platform.

still in contact with the ground. In the flying phase the driving unit and the leg both leave the ground. This motion is similar but it is not strictly a free falling motion due to friction.

Figure 4 is a mechanical diagram of the locomotion platform before the driving unit leaves the ground, that is, the bending phase. Here the driving unit remains stationary until F_y is large enough to lift the driving unit up and enter the lifting phase.

We considered that the leg bends slowly during the bending phase, so it can be regarded as a quasi-static process. In the figure, F_x, F_y, and M are the x-axial load, the y-axial load, and the moment from motor applied to the upper end of the leg, respectively. F_A and f_A are the normal force and friction force between the sliders and vertical slide ways. The coefficient of friction of F_A and f_A is μ_s, and G stands for the gravity of the driving unit. Thus, the dynamical equations of the driving unit are as shown below:

$$F_y + N_m = G + 2f_A, \tag{4}$$

$$2F_A h + f_m R = M, \tag{5}$$

$$f_m + 2F_A = F_x. \tag{6}$$

The compliant flipper-leg can be divided into two parts, the bending part of the leg and the straight part of the leg part II in figure 4 so that three large deflection equations can be applied. The straight part contacts the ground, while the bending part denotes the transforming part of the leg. The friction force f and normal force N between the leg and the ground are almost equal to F_x and F_y, and the moments are balance for the bending part are as listed below:

$$N(a + 0.5l_1) + fb = M, \tag{7}$$

where $l1$ is the length of the straight part, and the coefficient of friction between the leg and the round is defined as μ_d.

As analyzed before, the driving unit leaves the ground when the y-axial component of F_0 is larger than the weight of the unit, and then the lifting phase begins. In this phase the dynamical model of the driving unit can be modeled using the following equations:

$$F_x - 2F_A = m\ddot{x}, \tag{8}$$

$$-2f_A + F_y - mg = m\ddot{y}, \tag{9}$$

where m is the weight of the payload, $\ddot{x}$ and $\ddot{y}$ are the x axial and y axial accelerations, respectively. The bending of the leg is still regarded as a quasi-static process if the speed of rotation is low. The driving unit enters the flying phase when the length of the straight part becomes zero.

These equations are difficult to be solved due to the integral and second derivative. To solve equations (1)–(3) where the integral is involved, a searching method was used to look for solution within given errors. As for equations (8) to (9) that contained a second derivative, we used an iterative algorithm for this calculation.

2.4. Robot locomotion platform

A platform for a robot with four legs has also been developed to explore the performance of the compliant flipper-leg as a propulsion unit for a complete robot. This platform has four yellow compliant legs made from polyurethane, as shown in figure 5. The frame of this robot is 385 × 620 × 110 mm, and it weighs 11.3 kg. Yellow sponges are fixed to the bottom of the robot to absorb the shock when it collides with the floor to protect the mechanical structures, circuit boards and motors. When the robot is stationary on the floor, point C is 70 mm above the floor. Each leg is driven by a MAXON motor with an Elmo driving unit. The frame of the robot is assembled by 2020 aluminum profiles. The compliant leg is designed to be a simple rectangular block 315 mm long × 55 mm wide × 15 mm thick. Compared to RHex [31, 32] and AQUA [33] who possess six legs, the robot platform has only four flipper-legs with limited gaits. However, it is sufficient to obtain the locomotion performance of the compliant flipper-leg during the robot walking on terrains with four flipper-legs rotating synchronously. When the robot is turned on, the legs bend the motor drives the robot up and then propels it forward. In the experiment, the forward speeds, fluctuations in height, and the cost of transport (COT) were recorded to evaluate how well the robot performed. COT is a non-dimensional value to evaluate the consumption of energy as the animals propel themselves along, or the robots are transported [34]. COT is also widely used to study the cost of robot's energy during locomotion [35, 36]. Here COT is defined as shown below:

$$\mathrm{COT} = \frac{P_{\mathrm{i}}}{WV}. \tag{11}$$

P_{i} is the input power provided by the motor, which finally transforms to mechanical energy of robot and dissipates to air as fuel caused by material's viscosity. W is the gravity of the system, and V is the average forward speed of the robot. COT is calculated for an entire stride, which means the legs experience motion in all three phases, in a period defined as T. Since the output power of the motors changes during locomotion, P_{i} is defined as the mean output power of the motors that we record at a discrete time in a stride period T:

$$P_{\mathrm{i}} = \frac{\omega}{T}\sum_{T} M(t)\,\Delta t_{\mathrm{i}}, \tag{12}$$

where $M(t)$ means the output torque of the motor at time t, and Δt_{i} means the interval of time between two recorded torque values. By combining equations (11) and (12), COT is finally formed as shown below:

$$\mathrm{COT} = \frac{\omega\sum_{T} M(t)\,\Delta t_{\mathrm{i}}}{WVT}. \tag{13}$$

To calculate COT, we must obtain the robot's forward speed, and the motor's output torque and period of stride. We recorded the leg bending process and robot movement with a camera, so its forward speed and period time can be calculated. We obtained the motor's output torque by recording the current flowing through its coil, based on the relationship where the output torque is proportional to the current. Before commencing this experiment, a whiteboard with standardized grids, called a mask board, was erected along a red line marked on the rubber floor. We then used a camera to photograph the mask board and then use it as background. We then remove the mask board and allowed the robot to walk along the red line. This red line is to ensure that the mask board and one side of robot's leg would be in the same vertical plane, and thus eliminate any error caused by the visual angle of the camera. The camera also recorded the movement of the robot as a video with 30 frames per second. After finishing the experiment, we extracted every frame from the video, and overlaid them with the background photo. By reading the position of the output axle of the motor marked as point C in figure 5(a) on the mask board, we obtained the trajectories and length of stride at while the motor was at different speeds of rotation. The period of stride T is calculated from when the motor begins to rotate to when the robot falls down on the floor. Then its forward speed could be calculated using the length of stride and period of time. Every experiment was repeated three times under the same condition in order to obtain any errors.

3. Theoretical and experimental results

With the platforms and models now developed, we can examine and explore the locomotion of the compliant flipper-leg under various conditions.

3.1. Results of single-leg platform

Figure 6 shows the trajectories of the compliant flipper-leg at 0.5 rad s^{-1} speed of rotation in the simulations and experiments, respectively. The straight yellow bar represents the initial posture and position of the compliant flipper-leg, and the black dots represent the center of the motor's output axle. The trajectory can be divided into part I, part II and part III. The result shows that the two trajectories coincided well for part I and the simulated length of stride was almost the same as in the experiment. However, the trajectory from the simulation was higher than the experiment for part II, while part III was close to falling freely. Both trajectories actually fell quickly, but in the simulation the driving unit fell faster than the other one. This inconsistency between the two trajectories from the simulation and experiment occurred because (1) Polyurethane is not an ideal linear material because its elastic modulus decreases with a large strain. When the driving unit moves into part II, the trajectory from experiment is lower than

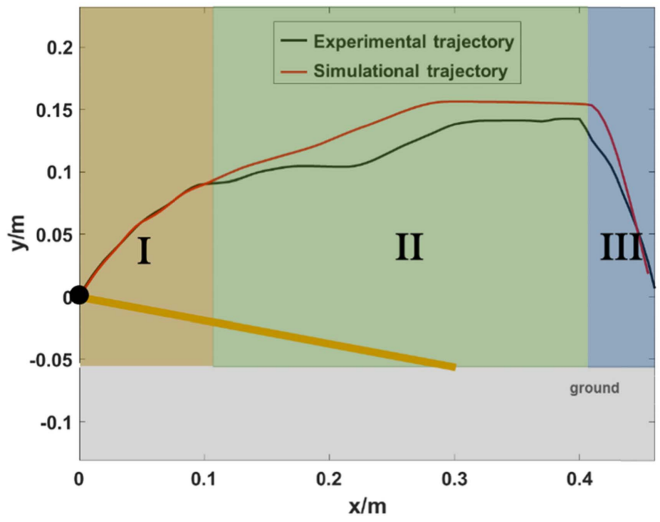

Figure 6. Trajectories of the compliant flipper-leg.

that from simulation in which material nonlinearity is ignored. (2) The inertial force of the legs was ignored because the weight of the leg is small and we assumed that the movement of legs would be quasi-static; (3) the coefficient between rubber material such as polyurethane and wooden ground may not be a constant value, an average measured value was used for the coefficient of friction. (4) Beside, friction and gaps between driving unit and vertical slide ways cause creep phenomenon in experiment, which leads to a creep phenomenon, further to a fluctuation and a lower trajectory. However, in simulation the coefficients of static friction and kinetic friction are set to be the same. Therefore, the creep phenomenon does not occur in simulation. Despite the small difference in the trajectory between the simulation and the experiment, we concluded that the mechanical model can basically reflect the locomotion dynamics of the compliant flipper-leg.

Based on the mechanical analysis of a single-leg locomotion platform, the trajectories, forward speed V_x and fluctuating height H of the driving unit were calculated with respect to five different rotation speeds ω of motor, as shown in figure 7.

Figure 7(a) shows the trajectories of the leg rotation axle during locomotion when the leg rotates at speeds of 0.5 rad s^{-1}, 1 rad s^{-1}, 2 rad s^{-1}, 3 rad s^{-1} and 4 rad s^{-1}, respectively. When the driving unit raised itself from the floor, the trajectories at lower rotating speeds of 0.5, 1 and 2 rad s^{-1} were similar. The trajectories at 0.5, 1 and 2 rad s^{-1} increased slowly until they were almost coincident at the first half part. These three trajectories also had a similar length of stride because the trajectory at 3 rad s^{-1} rises quickly and with a shorter length stride than those at lower rotating speeds. However, the trajectory at a rotating speed of 4 rad s^{-1} appears to be different because it rises very quickly and then drops down quickly; this was the shortest stride length in the trajectories at all five speeds. Figures 7(b) and (c) presents the forward speed, the COT, and fluctuations in the height of the locomotion platform, respectively. Here, the forward speed V_x increased from 0.5 to 3 rad s^{-1} and then decreased at 4 rad s^{-1}. The fluctuations in height decreased at 0.5 to 3 rad s^{-1} and then increased at 4 rad s^{-1}. The highest forward speed and lowest fluctuations in height are both at 3 rad s^{-1}. The dynamics of COT shows that it generally became larger at higher rotating speeds but experienced its lowest value at 2 rad s^{-1}. Moreover, COT changed slowly from 0.5 to 3 rad s^{-1}, and then went up quickly from 3 to 4 rad s^{-1}. So, if the motor is allowed to rotate faster, a higher forward speed can be obtained without sacrificing energy efficiency, and if the motor rotates very quickly, forward speed decreases and the energy efficiency drops quickly.

It can be concluded from the above that the motions at 0.5, 1, 2 and 3 rad s^{-1} were regular, but when ω was 4 rad s^{-1}, the motion was out of the order. The difference between trajectories at 4 rad s^{-1} and other rotating speeds is caused by the severe slippage. The theoretical analysis is based on assumption that the leg would not slip on ground for simplicity. However, the slippage actually happens when the flipper-leg rotates fast. And the slippage leads to a smaller a (displacement of driving unit along x-axial) and a larger l_1 (length of the straight part of the leg), and further a smaller component of F_0 in x-direction. As a result, the driving unit moves forward with a lower speed and a shorter stride length. Besides, COT that stands for energy efficiency increases quickly from 3 to 4 rad s^{-1} because severe slippage makes more energy dissipate.

3.2. Results of four-leg-robot platform

The robot locomotion platform allows the locomotion of the compliant flipper-leg to be examined

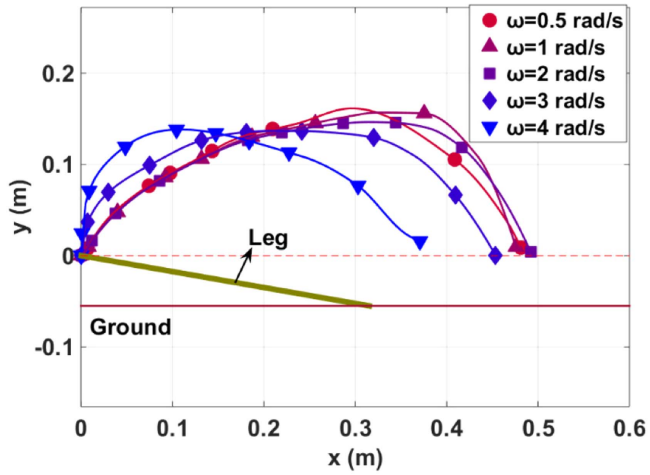

(a)

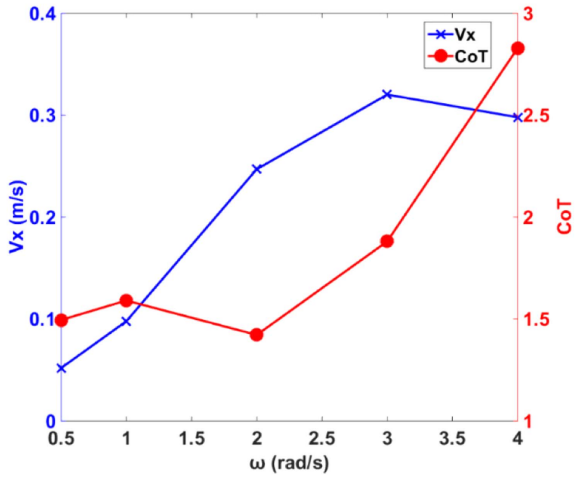

(b)

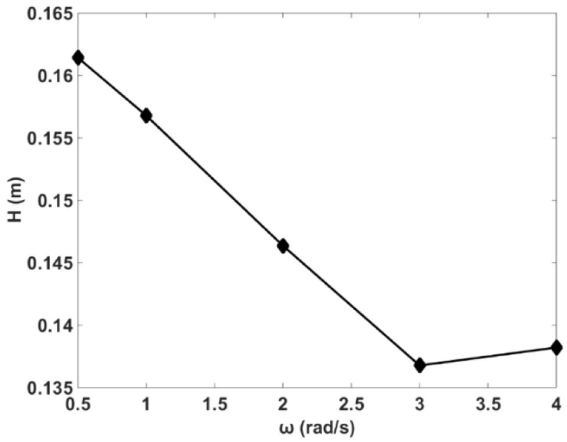

(c)

Figure 7. Simulation results of the single-leg locomotion platform.

experimentally. As mentioned before, we selected variable rotation speeds in the experiments. After considering the capability of the motors, a range of speed from 0.5 to 4 rad s^{-1} with just one stride was chosen for recording purposes. Their trajectories are shown in figure 8(a). All the trajectories are similar at 0.5, 1, 2 and 3 rad s^{-1}, but when the motor reached a rotating speed of 4 rad s^{-1}, the trajectory is obviously higher than others when x is around 0.1 m and the length of stride becomes shorter. So at low speeds, the speed at which the motor rotates is not an important factor of trajectory because it only begins to differ at higher speeds. The video shows that at low speeds, the legs of the robot did not slip on the ground, but once the speed of rotation increased, so too did slippage. In figure 8(c), fluctuations in the height of the robot

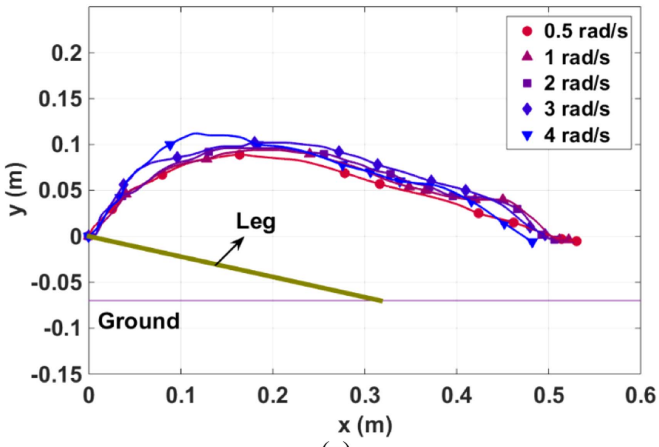

(a)

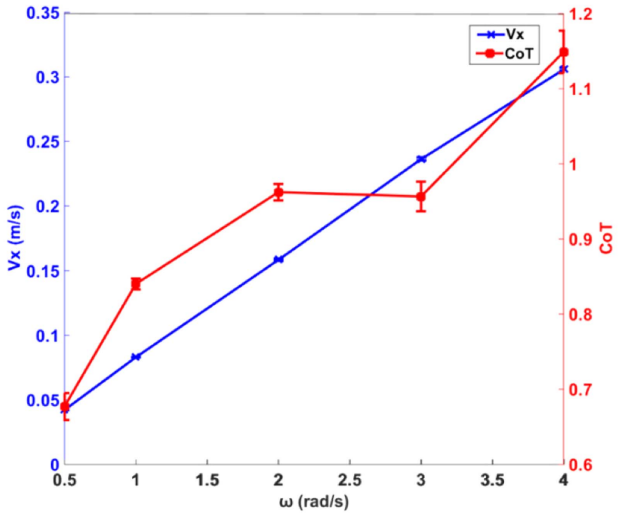

(b)

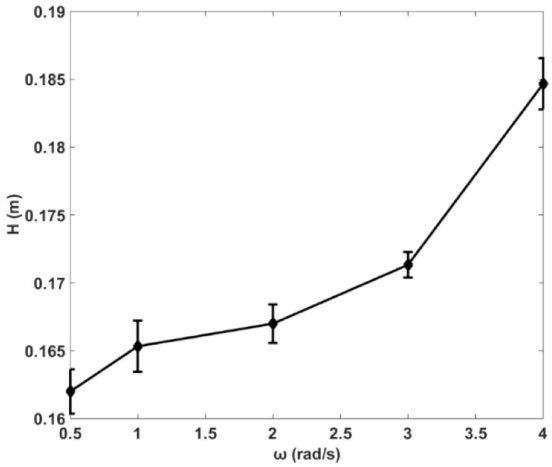

(c)

Figure 8. Experimental result of the robot locomotion platform.

increased slowly before reaching 3 rad s^{-1}, but from 3 to 4 rad s^{-1}, the height fluctuated faster due to slippage. Figure 8(b) shows that the robot's forward speed varied with COT at five speeds ranging from 0.5 to 4 rad s^{-1}. The chart representing forward speed shows that the forward speed V_x is strictly linear, and thus the forward speed of robots propelled by compliant legs on terrain is approximately proportional to the rotation speed of the motor. The proportional factor was 75.6 mm rad^{-1} s^{-1}, so the maximum forward speed can reach 0.3 m s^{-1} at 4 rad s^{-1}, which is 0.48 body lengths per second. Another chart in figure 8(b) shows the COT where As COT increased with almost all rotating speeds the

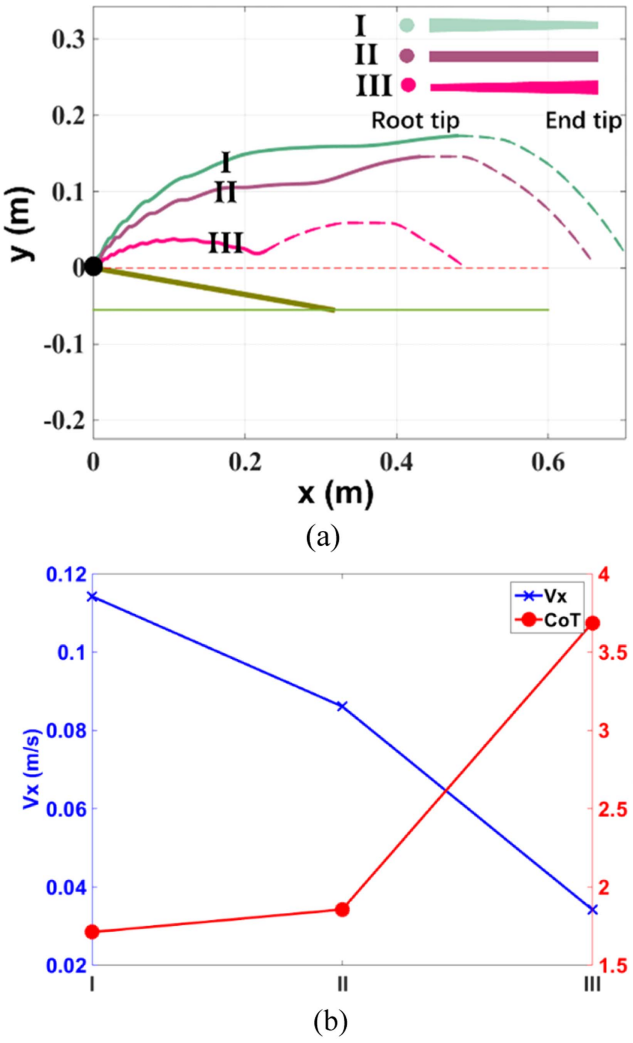

Figure 9. Special design of the complaint flipper-legs.

compliant leg experienced a subsequent decrease in its power efficiency. As with the fluctuations in height, COT rose faster from 3 to 4 rad s^{-1} because more energy dissipated in dynamical friction between the leg and the ground. Though a higher rotation speed leads to a higher forward speed, slippage occurs at this situation, which leads to a sharp decline of power efficiency.

3.3. Special design of compliant flipper-legs

Now that the mechanical model has been developed, the design of the complaint flipper-legs can be examined in order to obtain a high locomotion performance. By observing animals with compliant appendages, almost all legs have a slope from the root to the end tip, and the tip of the root is thicker than the tip at the end, just like leg I in figure 9(a). One typical example is the pectoral fins of mudskippers, an amphibious fish who excels to locomote in muddy substrates and swimming underwater with its compliant pectoral fins [37, 38]. In order to validate the advantages of a flipper-leg with such a shape, we constructed two different legs; one leg has the same thickness along its length, while the other was thinner at the root tip and thicker at the end tip. These two legs are called legs II and III, respectively, as shown in figure 9(a). Thus, we now have three leg shapes with different slopes, so the locomotion on terrain can now be compared.

We calculated the trajectories V_x, and COT based on a single-leg platform with three different legs, and presented the results in figures 9(a) and (b). The figure shows that leg I has the highest forward speed and the lowest COT, so a leg shaped like leg I was better than the other two. That leg I had the best performance coincides with the cases in nature, where for instance, fish are stiffer in their anterior region than at their posterior region, so leg I was better able to reproduce the kinematics of fish swimming freely [39]. The trajectory of leg III is lowest and has an obvious valley that was caused by energy accumulation and releasing as the compliant leg was bending. Since leg III has a thinner root tip and a strong end tip, when the leg begins to bend, more energy is stored in the root which causes

more the root to bend more, and that results in a lower trajectory. The stored energy is released when it enters the flying phase because the end tip is strong enough, and it has bent less and thus can generate more propulsive force, which let the driving unit go up obviously and then a valley appears.

3.4. Discussion

In the above section, we presented the results from simulations and experiments for a single-leg platform and experiments for four-leg-robot platform, including their trajectories, forward speed, fluctuations in height, and COT versus various output rotation speed of the motor unit.

It is necessary to point out why two different platforms were used to explore the performance of the compliant legs, and compare the results of two different platforms. The description of the single-leg platform in section 2.1 indicates that the horizontal load, including the vertical slide ways and some other parts, weight almost 12.36 kg, which is much larger than the 2 kg vertical load. There was no situation where a compliant leg was used in a robot, even though a a multiple-leg platform was necessary. However, a four-leg-robot platform is difficult to model because the two front legs have a different mechanical motion to the two back legs. We therefore used a single-leg platform to simulate a compliant flipper-leg, and a four-leg-robot platform to examine how this kind of flipper-leg would perform.

Although these two platforms were built for different purposes, there are still some interesting results from a comparison of locomotion. When the motion of the driving unit in the single-leg platform finishes its lifting phase and enters the flying phase, the shift of motion is more obvious than in four-leg-robot platform because the weight of vertical slide ways in the single-leg platform is enough to generate considerable inertia which causes the driving unit to quickly decelerate, and the leg slip on the ground easily. For that reason, the driving unit's length of stride decreases at a rotation speed of 4 rad s^{-1} compared to slower speeds. Alternatively, forward speed increases when speed of rotation of the robot's locomotion platform increased from 0.5 to 4 rad s^{-1}.

4. Conclusions

The purpose of this paper is to present a theoretical and experimental analysis of a compliant straight flipper-leg during terrestrial locomotion. Through the results from a single-leg and a four-leg-robot locomotion platform, we found that the best forward speed is linked to a certain rotation speed of the motor; if the motor rotates too fast, slippage between the leg and the ground occurs. To analyze propulsive efficiency, we calculated COT and found that a lower speed of rotation is better because once the legs slip on the floor, COT increases quickly. The locomotion performance of a four-leg robot reveals that these compliant legs can be applied to robots. Moreover, we compared three kinds of legs with different slopes and found that leg I performed best at forward speed and propulsive efficiency. Leg I has a slope where its thickness decreases from the root tip to the end tip, which is similar to animal appendages in nature, such as the pectoral fins of mudskippers.

The methods to obtain the experimental trajectories of compliant flipper-legs and analyze the dynamical behavior of compliant flipper-legs can be used to optimize the structure of the amphibious robot, and provide advice for the controlling strategies of the multi-flipper-leg robot with versatile gaits. Future work will focus on a theoretical and experimental exploration of compliant flipper-legs walking on other terrain such as soil and sand.

Acknowledgments

This research is supported by National Natural Science Foundation of China (No. 51375468, 11272303), ARC Discovery Grant (DP150102636) and the Fundamental Research Funds for the Central Universities of China (WK2090050026).

References

[1] Boxerbaum A S, Werk P, Quinn R D and Vaidyanathan R 2005 Design of an autonomous amphibious robot for surf zone operation: I. Mechanical design for multi-mode mobility *Proc. IEEE/ASME Int. Conf. on Advanced Intelligent Mechatronics, 2005 (July)* (IEEE) pp 1459–64

[2] Crespi A, Karakasiliotis K, Guignard A and Ijspeert A J 2013 Salamandra robotica II: an amphibious robot to study salamander-like swimming and walking gaits *IEEE Trans. Robot.* **29** 308–20

[3] Ijspeert A J, Crespi A, Ryczko D and Cabelguen J M 2007 From swimming to walking with a salamander robot driven by a spinal cord model *Science* **315** 1416–20

[4] Hirose S 1993 *Biologically Inspired Robots: Snake-Like Locomotors and Manipulators* (Oxford: Oxford University Press)

[5] Low K H, Zhou C, Ong T W and Yu J 2007 Modular design and initial gait study of an amphibian robotic turtle *IEEE Int. Conf. on Robotics and Biomimetics (ROBIO) (December 2007)* (IEEE) pp 535–40

[6] Liang X, Xu M, Xu L, Liu P, Ren X, Kong Z and Zhang S 2012 The amphihex: a novel amphibious robot with transformable leg-flipper composite propulsion mechanism *IEEE/RSJ Int. Conf. on Intelligent Robots and Systems (IROS) (October 2012)* (IEEE) pp 3667–72

[7] Zhang S, Liang X, Xu L and Xu M 2013 Initial development of a novel amphibious robot with transformable fin-leg composite propulsion mechanisms *J. Bionic Eng.* **10** 434–45

[8] Zhang S, Zhou Y, Xu M, Liang X, Liu J and Yang J 2016 AmphiHex-I: locomotory performance in amphibious environments with specially designed transformable flipper-legs *IEEE/ASME Trans. Mechatronics* **21** 1720–31

[9] Calisti M, Corucci F, Arienti A and Laschi C 2015 Dynamics of underwater legged locomotion: modeling and experiments on an octopus-inspired robot *Bioinspiration Biomimetics* **10** 046012

[10] Çulha U and Iida F 2016 Enhancement of finger motion range with compliant anthropomorphic joint design *Bioinspiration Biomimetics* **11** 026001

[11] Umedachi T, Vikas V and Trimmer B A 2016 Softworms: the design and control of non-pneumatic, 3D-printed, deformable robots *Bioinspiration Biomimetics* **11** 025001
[12] El Daou H, Salumäe T, Chambers L D, Megill W M and Kruusmaa M 2014 Modelling of a biologically inspired robotic fish driven by compliant parts *Bioinspiration Biomimetics* **9** 016010
[13] Park Y J, Huh T M, Park D and Cho K J 2014 Design of a variable-stiffness flapping mechanism for maximizing the thrust of a bio-inspired underwater robot *Bioinspiration Biomimetics* **9** 036002
[14] Kancharala A K and Philen M K 2014 Study of compliant fin and compliant joint stiffness on propulsive performance: theory and experiments *Bioinspiration Biomimetics* **9** 036011
[15] Kim H J, Song S H and Ahn S H 2013 A turtle-like swimming robot using a smart soft composite (SSC) structure *Smart Mater. Struct.* **22** 014007
[16] Otake M, Kagami Y, Inaba M and Inoue H 2002 Motion design of a starfish-shaped gel robot made of electro-active polymer gel *Robot. Auton. Syst.* **40** 185–91
[17] Li C, Zhang T and Goldman D I 2013 A terradynamics of legged locomotion on granular media *Science* **339** 1408–12
[18] Li C, Umbanhowar P B, Komsuoglu H, Koditschek D E and Goldman D I 2009 Sensitive dependence of the motion of a legged robot on granular media *Proc. Natl Acad. Sci. USA* **106** 3029–34
[19] Park H S and Sitti M 2009 Compliant footpad design analysis for a bio-inspired quadruped amphibious robot *IEEE/RSJ Int. Conf. on Intelligent Robots and Systems (IROS) (October 2009)* (IEEE) pp 645–51
[20] Xu L, Zhang S, Jiang N and Xu R 2015 A hybrid force model to estimate the dynamics of curved legs in granular material *J. Terramech.* **59** 59–70
[21] Raibert M H 1986 *Legged Robots That Balance* (Cambridge, MA: MIT Press)
[22] Ahmadi M and Buehler M 1997 Stable control of a simulated one-legged running robot with hip and leg compliance *IEEE Trans. Robot. Autom.* **13** 96–104
[23] Howell L L 2001 *Compliant Mechanisms* (New York: Wiley)
[24] Howell L L and Midha A 1995 Parametric deflection approximations for end-loaded, large-deflection beams in compliant mechanisms *J. Mech. Des.* **117** 156–65
[25] Park H S and Sitti M 2009 Compliant footpad design analysis for a bio-inspired quadruped amphibious robot *IEEE/RSJ Int. Conf. on Intelligent Robots and Systems (IROS) (October 2009)* (IEEE) pp 645–51
[26] Su H-J 2009 A pseudo-rigid body 3R model for determining large deflection of cantilever beams subject to tip loads *J. Mech. Robot.* **1** 021008
[27] Huang K J, Huang C K and Lin P C 2014 A simple running model with rolling contact and its role as a template for dynamic locomotion on a hexapod robot *Bioinspiration Biomimetics* **9** 046004
[28] Galloway K C, Clark J E and Koditschek D E 2013 Variable stiffness legs for robust, efficient, and stable dynamic running *J. Mech. Robot.* **5** 011009
[29] Xia K 2011 Finite element modeling of tire/terrain interaction: application to predicting soil compaction and tire mobility *J. Terramech.* **48** 113–23
[30] Ozaki S and Kondo W 2016 Finite element analysis of tire traveling performance using anisotropic frictional interaction model *J. Terramech.* **64** 1–9
[31] Saranli U, Buehler M and Koditschek D E 2000 Design, modeling and preliminary control of a compliant hexapod robot *Proc. ICRA'00 IEEE Int. Conf. on Robotics and Automation (2000)* vol 3 (IEEE) pp 2589–96
[32] Saranli U, Buehler M and Koditschek D E 2001 RHex: a simple and highly mobile hexapod robot *Int. J. Robot. Res.* **20** 616–31
[33] Dudek G *et al* 2007 Aqua: an amphibious autonomous robot *Computer* **40** 46–53
[34] Tucker V A 1975 The energetic cost of moving about: walking and running are extremely inefficient forms of locomotion. Much greater efficiency is achieved by birds, fish—and bicyclists *Am. Sci.* **63** 413–9
[35] Cao Q and Poulakakis I 2015 On the energetics of quadrupedal running: predicting the metabolic cost of transport via a compliant-torso model *Bioinspiration Biomimetics* **10** 056008
[36] Seok S, Wang A, Chuah M Y, Otten D, Lang J and Kim S 2013 Design principles for highly efficient quadrupeds and implementation on the MIT Cheetah robot *IEEE Int. Conf. on Robotics and Automation (ICRA) (May 2013)* pp 3307–12
[37] Wang L, Xu M, Liu B, Jiang T, Zhang S and Yang J 2013 Experimental study on morphology and kinematics of mudskipper in amphibious environments *IEEE Int. Conf. on Robotics and Biomimetics (ROBIO) (May 2013)* (IEEE) pp 1095–100
[38] Pace C M and Gibb A C 2009 Mudskipper pectoral fin kinematics in aquatic and terrestrial environments *J. Exp. Biol.* **212** 2279–86
[39] Kelsey N *et al* 2015 Effects of non-uniform stiffness on the swimming performance of a passively-flexing, fish-like foil model *Bioinspiration Biomimetics* **10** 056019